electronic reprint

JOURNAL OF APPLIED CRYSTALLOGRAPHY

ISSN: 1600-5767
journals.iucr.org/j

Extending the single-crystal quartz pressure gauge up to hydrostatic pressure of 19 GPa

Katharina S. Scheidl, Alexander Kurnosov, Dmytro M. Trots, Tiziana Boffa Ballaran, Ross J. Angel and Ronald Miletich

J. Appl. Cryst. (2016). **49**, 2129–2137

JOURNAL OF APPLIED CRYSTALLOGRAPHY

ISSN 1600-5767

Extending the single-crystal quartz pressure gauge up to hydrostatic pressure of 19 GPa

Katharina S. Scheidl,[a]* Alexander Kurnosov,[b] Dmytro M. Trots,[b] Tiziana Boffa Ballaran,[b] Ross J. Angel[c] and Ronald Miletich[a]

[a]Department of Mineralogy and Crystallography, University of Vienna, Althanstrasse 14, Vienna, 1090, Austria, [b]Bavarian Research Institute of Experimental Geochemistry and Geophysics, University of Bayreuth, Universitätsstrasse 30, Bayreuth, 95447, Germany, and [c]Department of Geosciences, University of Padua, Via G. Gradenigo 6, Padua, 35131, Italy. *Correspondence e-mail: katharina.sarah.scheidl@univie.ac.at

Received 9 June 2016
Accepted 29 September 2016

Edited by K. Chapman, Argonne National Laboratory, USA

Keywords: quartz; internal diffraction standards; high pressure; equations of state; diamond-anvil cells; pressure media.

Supporting information: this article has supporting information at journals.iucr.org/j

In situ high-pressure diffraction experiments on single-crystal α-quartz under quasi-hydrostatic conditions up to 19 GPa were performed with diamond-anvil cells. Isotropic pressures were calibrated through the ruby-luminescence technique. A 4:1 methanol–ethanol mixture and the densified noble gases helium and neon were used as pressure media. The compression data revealed no significant influence of the pressure medium at room temperature on the high-pressure behavior of α-quartz. In order to describe its compressibility for use as a pressure standard, a fourth-order Birch–Murnaghan equation of state (EoS) with parameters $K_{T0} = 37.0$ (3) GPa, $K'_{T0} = 6.7$ (2) and $K''_{T0} = -0.73$ (8) GPa^{-1} was applied to fit the data set of 99 individual data points. The fit of the axial compressibilities yields $M_{T0} = 104.5$ (8) GPa, $M'_{T0} = 13.7$ (4), $M''_{T0} = -1.04$ (11) GPa^{-1} (a axis) and $M_{T0} = 141$ (3) GPa, $M'_{T0} = 21$ (2), $M''_{T0} = 8.4$ (6) GPa^{-1} (c axis), confirming the previously reported anisotropy. Assuming an estimated standard deviation of 0.0001% in the quartz volume, an uncertainty of 0.013 GPa can be expected using the new set of EoS parameters to determine the pressure.

1. Introduction

The determination and monitoring of pressure are essential in performing successful high-pressure experiments. Nowadays, the majority of typical *in situ* experiments to measure crystallographic data by applying spectroscopic methods and diffraction techniques are performed using the diamond-anvil cell (DAC) technique. Inside the pressure chamber of a DAC, the sample crystals are exposed to a dense fluid providing a homogeneous stress distribution and thus representing quasi-hydrostatic conditions (*e.g.* Angel *et al.*, 2007; Dewaele & Loubeyre, 2007; Klotz *et al.*, 2009).

Pressures are usually derived using a well calibrated reference material, which is loaded in addition to the sample inside the pressure chamber. All these reference materials are characterized by a physical quantity that changes with pressure. Pressure gauges based on laser-induced luminescence techniques, *e.g.* ruby, Sm:SrB_4O_7 and Sm:YAG (YAG is yttrium aluminium garnet) (Mao *et al.*, 1986; Datchi *et al.*, 1997; Trots *et al.*, 2013), are suitable for spectroscopic studies at room temperature and non-ambient temperatures and are convenient for recording of pressure on short time scales within seconds. On the other hand, internal diffraction standards, *e.g.* Au, Pt, Pd, CaF_2, NaCl, MgO, Ne and SiO_2 (quartz) (Ming *et al.*, 1983; Angel, 1993; Knittle, 1995; Angel *et al.*, 1997; Dorfman *et al.*, 2012), have been rising in popularity for the determination of absolute pressure values.

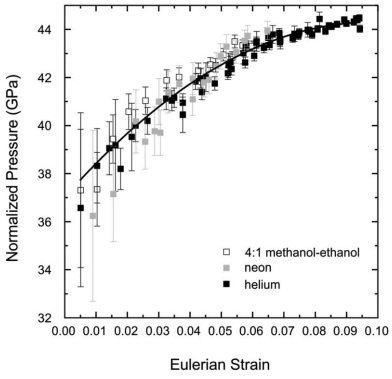

α-Quartz, which exhibits all the required properties of an internal diffraction standard (Hazen & Finger, 1981), was calibrated up to about 9 GPa by Angel *et al.* (1997) and established as a widely used pressure sensor within the hydrostatic limits of the most popular pressure medium, methanol–ethanol 4:1 (Angel *et al.*, 2007). Owing to its high relevance in geosciences, the high-pressure behavior of α-quartz is experimentally well established (*e.g.* Jayaraman *et al.*, 1987; Glinnemann *et al.*, 1992; Williams *et al.*, 1993; Kim-Zajonz *et al.*, 1999). SiO_2 crystallizes under ambient conditions in the trigonal polymorph α-quartz (space-group symmetry $P3_121$ or $P3_221$). It is thermodynamically stable up to about 3 GPa (Böhler & Arndt, 1974) and persists up to 21 GPa in a metastable state. Ahead of the pressure-induced gradual amorphization process, which has been reported above 25 GPa under room-temperature conditions (Hemley *et al.*, 1988; Kingma, Meade *et al.*, 1993), a structural transformation occurs at 21 GPa into a new phase, quartz II, with a still unknown structure (Kingma, Hemley *et al.*, 1993). First-principles calculations suggest that an elastic instability is responsible for the structural instability causing the transformation and the subsequent amorphization (Binggeli & Chelikowsky, 1992; Binggeli *et al.*, 1994; Gregoryanz *et al.*, 2000; Choudhury & Chaplot, 2006). The outlined transformation pathway of α-quartz has turned out to be sensitive to shear stresses and stress rates. Kingma, Meade *et al.* (1993) report the modified onset of the amorphization process to lower pressures under non-hydrostatic pressure conditions. When α-quartz is rapidly compressed in 10 s up to 45 GPa under hydrostatic conditions it transforms to a monoclinic $P2_1/c$ post-quartz phase (Haines *et al.*, 2001).

Numerous experimental studies both under atmospheric conditions and at elevated pressure focusing on the acoustic properties and the elastic behavior of α-quartz have been conducted by means of ultrasonic measurements (McSkimin *et al.*, 1965; Wang *et al.*, 1992; Heyliger *et al.*, 2003; Calderon *et al.*, 2007; Tarumi *et al.*, 2007), Brillouin spectroscopy (Gregoryanz *et al.*, 2000; Lakshtanov *et al.*, 2007; Wang *et al.*, 2015) and diffraction methods (McWhan, 1967; Jorgensen, 1978; d'Amour *et al.*, 1979; Levien *et al.*, 1980; Hazen *et al.*, 1989; Angel *et al.*, 1997; Kim-Zajonz *et al.*, 1999). Experimentally determined values of the bulk modulus $K_{T0} = -V_0(\delta P/\delta V)_{P=0}$, a quantity expressing the resistance to uniform compression, reveal a variation between 34 and 38 GPa, and values of its pressure derivative $K'_{T0} = (\delta K/\delta P)_{P=0}$ range between 5.4 and 6.3. These values are inconsistent with simulations based on density functional theory (Chelikowsky *et al.*, 1991; Di Pomponio & Continenza, 1993; Hamann, 1996; Demuth *et al.*, 1999; Holm & Ahuja, 1999; Kimizuka *et al.*, 2007). The measurement of pressure–volume data sets and the subsequent fit of equation-of-state (EoS) parameters are all restricted to hydrostatic pressure conditions up to about 13 GPa. As gas-loading techniques have been established in recent years and have become a standard procedure for preparing DAC sample loadings, the pressure media helium and neon have been widely used. These densified noble gases significantly expand the pressure regime of ideal hydrostaticity and enable high-pressure crystallographic investigations far beyond the hydrostatic limit of conventional pressure media such as the standard 4:1 methanol–ethanol mixture (Piermarini *et al.*, 1973; Bell & Mao, 1981).

However, the mono-atomic noble-gas species not only interpenetrate nanoporous open framework structures (Lv *et al.*, 2012; Hazen, 1983; Hazen & Finger, 1984; Talyzin *et al.*, 2009; Lee *et al.*, 2002; Perottoni & da Jornada, 1997; Nakano *et al.*, 1998; Talyzin & Luzan, 2010; Yagi *et al.*, 2007; Haines *et al.*, 2010) but also intercalate into compact structures (*e.g.* the high-temperature modification of SiO_2 cristobalite; Sato *et al.*, 2013), influencing phase transitions and the compressibility behavior. Thus, the question arises whether the tetrahedral framework of quartz is also a candidate structure with the ability to store individual noble-gas atoms on extra-framework interstitial positions and, consequently, to develop elastic stiffening and decrease compressibility. Considering the application of α-quartz as a pressure standard, we focus in this study on its elastic properties under pressure, in order to evaluate any effect of different pressure media close to the reported pressure of its structural instability. Measurements of pressure–volume data sets by means of high-precision single-crystal X-ray diffraction were carried out to record the compressibility of quartz in the commonly used pressure media helium, neon and a 4:1 methanol–ethanol mixture. Standard ruby was used as reference for the pressure determination. Compared to the relatively open framework of α-quartz (Le Page & Donnay, 1976), the dense structure of hexagonal close-packed oxygen atoms in ruby (*i.e.* Cr^{3+}-doped Al_2O_3; Lewis *et al.*, 1982) is supposed to show no or negligible interaction with the pressure media.

2. Experimental

The high-pressure experiments were carried out using the DAC technique. The sample materials used for this study were a commercial quartz oscillator in X-cut orientation [*i.e.* cut parallel to the $(11\bar{2}0)$ plane direction], double-side polished down to ~40 µm, and a natural untwinned quartz crystal in Y-cut orientation parallel to its natural $(10\bar{1}0)$ face, double-side polished down to ~20 µm. Both crystal orientations allow measurement of the *a* and *c* axes to almost equal resolution, resulting in a higher precision of the lattice parameter determination and, moreover, providing a verification of the absence of any significant shear-stress contributions under non-hydrostatic conditions. Fragments of approximately 50 × 80 µm in lateral size were cut off and mounted parallel to the 600 µm culet face of the DAC. As pressure sensor we used Cr^{3+}:Al_2O_3 (ruby) spheres (Chervin *et al.*, 2001) or natural ruby crystals from Burma in (0001) and $(11\bar{2}0)$ orientation polished down to 40 µm (as described by Schuster *et al.*, 2010). The sample and pressure standard were loaded into the spark-eroded boreholes of the gasket. A 4:1 mixture of methanol–ethanol, neon and helium were used as pressure-transmitting media, which are reported to remain hydrostatic up to 10.5, 16 and 60–70 GPa, respectively (Piermarini *et al.*, 1973; Bell & Mao, 1981; Klotz *et al.*, 2009). The densified neon and helium

Table 1
Details of the high-pressure sample loadings used for the individual experimental runs.

ETH = ETH-type DAC (Miletich *et al.*, 2000); BGI = BGI-designed DAC (Kantor *et al.*, 2012). ME = 4:1 methanol–ethanol mixture. BoeAl = Boehler–Almax anvils (Boehler & de Hansetters, 2004).

Run	DAC	Anvil type	Gasket material	Borehole ∅/height (μm)	Quartz orientation	Ruby	Pressure medium	Diffractometer	P_{max} (GPa)
#1	ETH	BoeAl	Steel	300/100	$(11\bar{2}0)$	Platelets	ME	Huber 5042	10.64
#2	ETH	Standard	Steel	300/100	$(11\bar{2}0)$	Platelets	He	Stoe AED2	12.40
#3	ETH	Standard	Steel	300/100	$(10\bar{1}0)$	Sphere	He	Stoe AED2	19.17
#4	BGI	BoeAl	Re	250/60	$(10\bar{1}0)$	Sphere	He	Huber 5042† BGI	15.81
#5	BGI	BoeAl	Re	250/60	$(10\bar{1}0)$	Sphere	Ne	Huber 5042† BGI	11.57
#6	BGI	BoeAl	Re	250/60	$(10\bar{1}0)$	Sphere	Ne	Huber 5042† BGI	9.17

† Trots *et al.* (2011).

gases were loaded into the pressure chamber of the DACs using the gas-loading system as described by Kurnosov *et al.* (2008). A summary of the experimental details of the individual sample loadings of the various run series (#1 to #6) is provided in Table 1.

Luminescence spectra of the ruby samples were recorded by employing either a Horiba LabRam-HR 800 Raman spectrometer using the emission of a 532 nm laser (runs #1 to #3) or a Horiba LabRam-HR 300 Raman spectrometer using the emission of a 632.8 nm laser (runs #4 to #6). A grating with 1800 grooves per millimetre was set. An Olympus 50× long-working-distance objective (numerical aperture = 0.5) was used. The calibration of the systems was done using the Raleigh line, resulting in a wavenumber accuracy better than 0.5 cm^{-1}. The luminescence spectra recorded in the range between 690 and 700 nm were measured with an exposure time of 1 s. To extract precise band positions, the recorded luminescence bands were fitted after subtracting background and assuming Lorentzian–Gaussian band shapes with the program *PeakFit 4* (Systat Software, 2007) by applying the Gauss–Lorentz area method.

Pressure values were obtained by means of the laser-induced luminescence technique following the calibration for the R_1 line shift as reported by Jacobsen *et al.* (2008). In order to determine the pressure-dependent line shift, the spectra of the ruby samples were measured at atmospheric pressure and the position of the R_1 luminescence line was used as the reference. Temperature fluctuations made it necessary to apply statistical tests in order to check the significance of analytically determined standard deviations. Averaging multiply repeated measurements yields an estimated standard deviation of ±0.05 GPa for the Horiba LabRam-HR 800 spectrometer and ±0.10 GPa for the Horiba LabRam-HR 300 spectrometer.

High-pressure Raman spectra of quartz were collected for runs #1, #2 and #3 up to 20.79 GPa in order to observe the variation of the spectra with pressure and to monitor the evolution of the full widths at half-maxima (FWHMs) of the individual vibrational modes (see supplementary material). The Horiba LabRam-HR 800 spectrometer was therefore used with the same settings mentioned above. The spectra were accumulated in the range 90–600 cm^{-1} with a measuring time of 60 s.

Single-crystal X-ray diffraction measurements of the quartz crystals up to 19.31 GPa were performed on three different four-circle diffractometers. The Huber 5042 diffractometer (run #1) and the Stoe AED2 diffractometer (runs #2 and #3) are equipped with a full Eulerian cradle capable of being operated in the eight-position centering mode (Hamilton, 1974) and non-monochromated conventional sealed-tube sources (Mo radiation, λ = 0.7093 Å). The Huber 5042 BGI Eulerian cradle single-crystal diffractometer (runs #4 to #6) is coupled with an ultra-high-intensity rotating anode X-ray source from Rigaku and equipped with multilayer Varimax focusing optics (Mo $K\alpha$ radiation) (Trots *et al.*, 2011). All diffractometers are operated with the *SINGLE* software (Angel & Finger, 2011). From 10 to 20 non-equivalent Bragg peaks in the accessible part of the reciprocal space between 9 and 34° 2θ were measured by employing the eight-position centering technique to evaluate the precise lattice parameters by applying symmetry-constrained vector least-squares refinement to the recorded setting angles. The measured values and uncertainties of the resulting lattice parameters and unit-cell volumes of quartz are listed in supplementary Table S1, together with the pressure derived from recorded line positions of the ruby luminescence signals.

The EoS parameters were fitted by least squares to the data points following the Birch–Murnaghan formalisms (Birch, 1947) using the software *EoSFit7* (Angel *et al.*, 2014).

3. Results

The peak widths of the quartz Bragg intensities were monitored with respect to the FWHM of the ruby R_1 luminescence line. Throughout the complete measured pressure range up to the maximum pressure of 20.79 GPa the value of the FWHM of the R_1 line does not change significantly and reveals ideal hydrostatic conditions for the sample loadings. In contrast, the quartz Bragg peaks began to broaden under the verifiable hydrostatic conditions at approximately 18.7 GPa. Above 19.3 GPa it was not possible to measure the unit-cell parameters by X-ray diffraction owing to significant broadening of the Bragg reflections and recognizable changes of the optical and morphological properties of the crystal, *i.e.* physical disintegration. These observations confirm the beginning of structural changes. However, it was possible to collect Raman

spectra up to at least 20.79 GPa. The Raman modes can be assigned to the reported modes of quartz (*e.g.* Scott & Porto, 1967). The Raman spectra did not indicate any significant change that could be attributed to a structural phase transition.

Within the verified hydrostatic conditions of the six individual sample loadings, 99 data points were collected in total (16 in 4:1 methanol–ethanol mixture, 20 in neon and 57 in helium, and 6 at 10^{-4} GPa in air; see Table S1). The average standard uncertainty (s.u.) of the volume data is about 0.001% (ranging from 0.006 to 0.0005%). As the measurements were performed on three different diffractometers, all unit-cell parameters were normalized relative to those obtained at 10^{-4} GPa of run #1, applying

$$V_{p\#i(\mathrm{norm})} = V_{p\#i} V_{0(\#1)}/V_{0(\#i)} \quad (1)$$

with p = individual data point and i = run number. Values at atmospheric pressure are denoted by a subscript 0. Owing to aberrations of different diffractometers, the absolute values of V_0 may vary; however, the ratio of V_0/V at a given pressure is the same for each instrument. So, this normalization is an appropriate way to merge data sets measured on different diffractometers. Run #1 was chosen as the reference because it is in excellent agreement with reported values of quartz at ambient conditions (Le Page & Donnay, 1976; Glinnemann *et al.*, 1992; Angel *et al.*, 1997). This approach to scale the runs with respect to one set as reference was chosen in order to preserve the absolute magnitude of uncertainties for the further data evaluation.

The pressure dependence of the unit-cell volume and the normalized lattice parameters a/a_0 and c/c_0 of the complete data set referenced to run #1 are plotted in Figs. 1 and 2. Fig. 3 shows the Eulerian strain f *versus* normalized pressure F_E. All plots (Figs. 1–3) reveal a uniform distribution of the data within their s.u. without any recognizable diversity of the data subsets assigned to different pressure media, showing that the choice of the pressure medium does not influence the compression behavior. Consequently, the further evaluation of the compressibility curves was achieved through analyzing the merged data sets #1 to #6.

The EoS parameters V_0, $K_{T0} = -V_0(\delta P/\delta V)_{P=0}$, $K'_{T0} = (\delta K/\delta P)_{P=0}$ and $K''_{T0} = (\delta^2 K/\delta P^2)_{P=0}$ of the volume, and x_0 (= a_0 or c_0), $M_{T0} = -x_0(\delta P/\delta x)_{P=0}$, $M'_{T0} = (\delta M/\delta P)_{P=0}$ and $M''_{T0} = (\delta^2 M/\delta P^2)_{P=0}$ of the axes were determined by fitting to the P–V, P–a and P–c data using the fourth-order Birch–Murnaghan (BM-4) EoS formalism (the subscript T denotes isothermal bulk and axial moduli). The results of the fits are summarized in Table 2. Up to 19 GPa, the quartz volume decreases by 23%

Table 2
EoS parameters of α-quartz resulting from fits of the unit-cell volume V and the lattice parameters a and c to the corresponding third-order Birch–Murnaghan (BM-3) and fourth-order Birch–Murnaghan (BM-4) EoS formalism.

	V_0 (Å^3)	K_{T0} (GPa)	K'_{T0}	K''_{T0} (GPa^{-1})	χ^2_w	$\lvert P_{obs} - P_{calc}\rvert_{max}$ (GPa)
BM-3	112.967 (4)	40.1 (2)	4.80 (4)	[−0.133]†	2.02	0.268
BM-4	112.968 (3)	37.0 (3)	6.7 (2)	−0.73 (8)	1.02	0.145

	a_0 (Å)	M_{T0} (GPa)	M'_{T0}	M''_{T0} (GPa^{-1})	χ^2_w	$\lvert P_{obs} - P_{calc}\rvert_{max}$ (GPa)
BM-4	4.91298 (11)	104.5 (9)	13.7 (4)	−1.04 (11)	1.16	0.156

	c_0 (Å)	M_{T0} (GPa)	M'_{T0}	M''_{T0} (GPa^{-1})	χ^2_w	$\lvert P_{obs} - P_{calc}\rvert_{max}$ (GPa)
BM-4	5.40430 (12)	141 (3)	21 (2)	8.4 (6)	1.46	0.29

† Implied value.

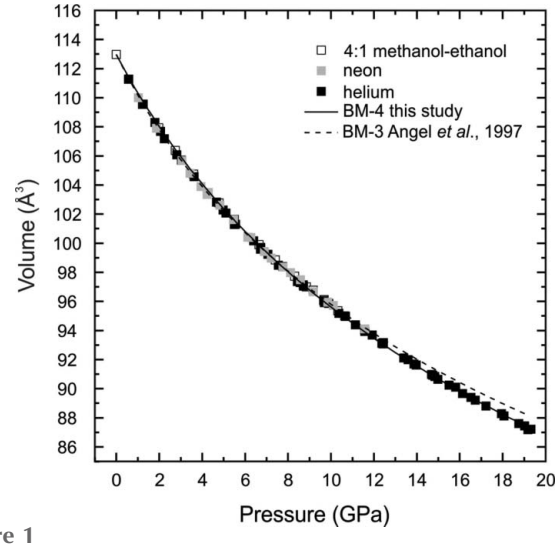

Figure 1
Variation of the unit-cell volume of α-quartz as a function of pressure. The solid line represents the result of the fit according to the applied fourth-order Birch–Murnaghan equation of state (BM-4) with the parameters provided in Table 2. The dashed line represents the calculated volume variation following the EoS truncated to BM-3 reported by Angel *et al.* (1997).

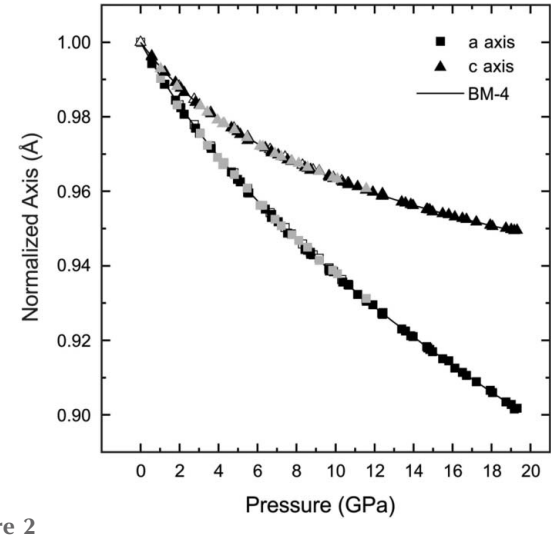

Figure 2
Variation of the normalized a and c axes (a/a_0 and c/c_0) as a function of pressure. Symbols of the different pressure media correspond to those used in Fig. 1. Solid lines represent the result of the fit according to the applied fourth-order BM EoS with the moduli provided in Table 2.

relative to its original volume at ambient pressure (Fig. 1). The compression of the trigonal quartz unit cell is highly anisotropic (see Fig. 2), as already reported by Angel *et al.* (1997), with a 10% decrease along the *a* axis, while the *c* axis decreases only by 5% over the entire pressure range of this study.

4. Discussion

Attempts to fit the current data set with a third-order Birch–Murnaghan (BM-3) EoS in analogy to the analysis performed by Angel *et al.* (1997) revealed results with evident deviations (see Table 2), which encompass (i) a much higher value for the bulk modulus K_{T0} than reported for any of the recent investigations (see references in Table 3); (ii) a significantly smaller value for K'_{T0} in comparison to those averaging between 5.9 and 6.4; (iii) a conspicuous high value for the goodness of fit $\chi^2 = 2.02$; and (iv) $|P_{obs} - P_{calc}|$ misfits up to 0.268 GPa, which are approximately 3–5 times larger than the s.u. of the *P* determination.

As the fit of a BM-3 EoS formalism apparently does not describe the data sufficiently, we fitted a BM-4 EoS, which includes apart from K'_{T0}, the first derivative of the bulk modulus with respect to pressure $(\delta K/\delta P)_{P=0}$, also the second derivative $K''_{T0} = (\delta^2 K/\delta P^2)_{P=0}$. The corresponding fit of the EoS parameters (*cf.* Table 2) matches the observed *P*–*V* data (see solid black line in Fig. 1). The fitted value of K''_{T0} differs significantly from the implied value of K''_{T0} of the BM-3 EoS. The application of the BM-4 EoS reduces the weighted goodness of fit χ^2_w and the maximal misfit in pressure $|P_{obs} - P_{calc}|$ significantly. The fact that the values of $|P_{obs} - P_{calc}|$ are of the order of the s.u. values of individual data points, together with the fact that the calculated V_0 is identical to the experimentally measured V_0, indicates that the parameters K_{T0}, K'_{T0} and K''_{T0} obtained by a BM-4 EoS represent the measured data quite well. Moreover, the plot of the normalized pressure *versus* the finite Eulerian strain (Fig. 3) shows an obvious parabolic shape, indicating the necessity of K''_{T0} to describe the compressibility behavior adequately.

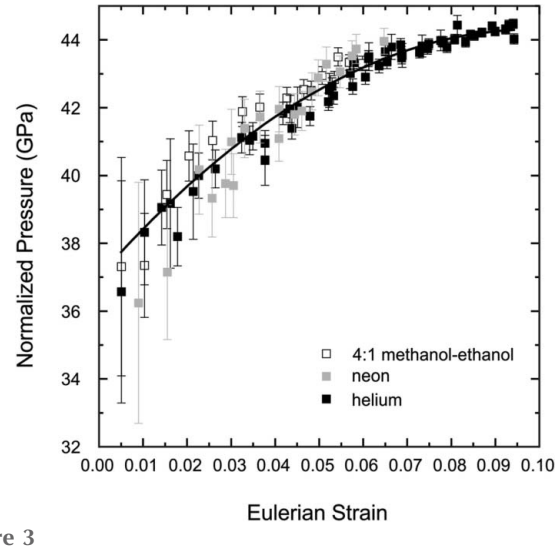

Figure 3
Normalized pressure as a function of Eulerian strain. Symbols indicating the different pressure media correspond to those used in Fig. 1. The solid line represents the fit of the fourth-order Birch–Murnaghan equation of state (BM-4).

Table 3
Isothermal bulk moduli K_{T0} and their pressure derivatives K'_{T0} of α-quartz at room pressure and temperature.

n.d. = not determined.

Author	Method	K_{T0} (GPa)	K'_{T0}	P_{max} (GPa)
McSkimin *et al.* (1965)	Ultrasonic measurement	37.15†	6.3	0.21
McWhan (1967)	X-ray diffraction	37.12	6.33	15
Jorgensen (1978)	Neutron scattering	36.4 (5)	6.3	2.5
d'Amour *et al.* (1979)	X-ray diffraction	36.5 (9)	5.9 (4)	6.8
Levien *et al.* (1980)	X-ray diffraction	37.1 (2)	6.2 (1)	6.1
Hazen *et al.* (1989)	X-ray diffraction	34 (4)	5.7 (9)	15
Wang *et al.* (1992)	Ultrasonic measurement	36.27 (3)†	5.6	0
Angel *et al.* (1997)	X-ray diffraction	37.12 (9)	5.99 (4)	8.9
Kim-Zajonz *et al.* (1999)	X-ray diffraction	38.7 (3)	5.2 (1)	13
Heyliger *et al.* (2003)	Ultrasound spectroscopy	37.17†	n.d.	0
Choudhury & Chaplot (2006)	Density functional theory‡	38.33†	n.d.	0
Calderon *et al.* (2007)	Ultrasonic measurement	37.28 (2)†	4.7 (5)	1
Kimizuka *et al.* (2007)	Density functional theory‡	34.20†	n.d.	20
Lakshtanov *et al.* (2007)	Brillouin spectroscopy	37.41†	n.d.	0
Tarumi *et al.* (2007)	Ultrasound spectroscopy	37.12†	n.d.	0
Wang *et al.* (2015)	Brillouin spectroscopy	37.26 (6)†	6.2 (2)	10
This study	X-ray diffraction	37.0 (3)	6.7 (2)	19.3

† The isothermal bulk modulus is derived from $K_T = K_S(\text{Reuss})/\{1 + \alpha_V^2[K_S(\text{Reuss})/C_P]T\}$, with $\alpha_V = 3.46 \times 10^{-5}$ K^{-1} obtained by fitting the data of Carpenter & Salje (1998) and $C_P = 0.00194$ GPa K^{-1}, derived from $C_P = 746.3$ (1) J kg^{-1} K^{-1} (Hemingway, 1987). The adiabatic bulk modulus K_S(Reuss) is calculated from the given C_{ij} by $1/(K_S - C_{13}) = 1/(C_{11} - C_{66} - C_{13}) + 1/(C_{33} - C_{13})$. ‡ Zero temperature.

The room-pressure BM-4 EoS parameters for both the volume compressibility and the *a* and *c* unit-cell axes fitted to the data of this study lie in between values reported in the literature (Tables 3 and 4). They are equivalent within their uncertainties to the most recent values reported by Wang *et al.* (2015), obtained through Brillouin spectroscopy. Figs. 4(*a*), 5(*a*) and 6(*a*) show that the volume and axial bulk moduli reported by Wang *et al.* (2015) at high pressure are in good agreement with the high-pressure data of this study.

Comparing the experimental data with the EoS parameters calculated by Angel *et al.* (1997) (dashed line in Fig. 1), at pressures above ∼8 GPa the fit noticeably starts to diverge from the measured *P*–*V* data of this study. The bulk moduli [$K_{T0} = 37.0$ (3) GPa of this study *versus* $K_{T0} = 37.12$ (9) GPa reported by Angel *et al.* (1997)] are identical within the s.u. values; the parameter K'_{T0} of this study is slightly larger [$K'_{T0} = 6.7$ (2) *versus* 5.99 (4)]. Between 2.5 and 6.5 GPa, the use of the new EoS parameters yields pressure values that are up to 0.0290 (4) GPa greater than the values from Angel *et al.* (1997). Above 7 GPa the discrepancy increases rapidly, with the new EoS giving values 0.100 (12) GPa less at 10 GPa and 1.400 (12) GPa less at 19 GPa (Fig. 7).

Figs. 4 and 5 show the different compressibility behavior of the crystallographic *a* and *c* axes. The linear modulus M_{aT} of the *a* axis follows a smooth curvature (Fig. 4*a*), which

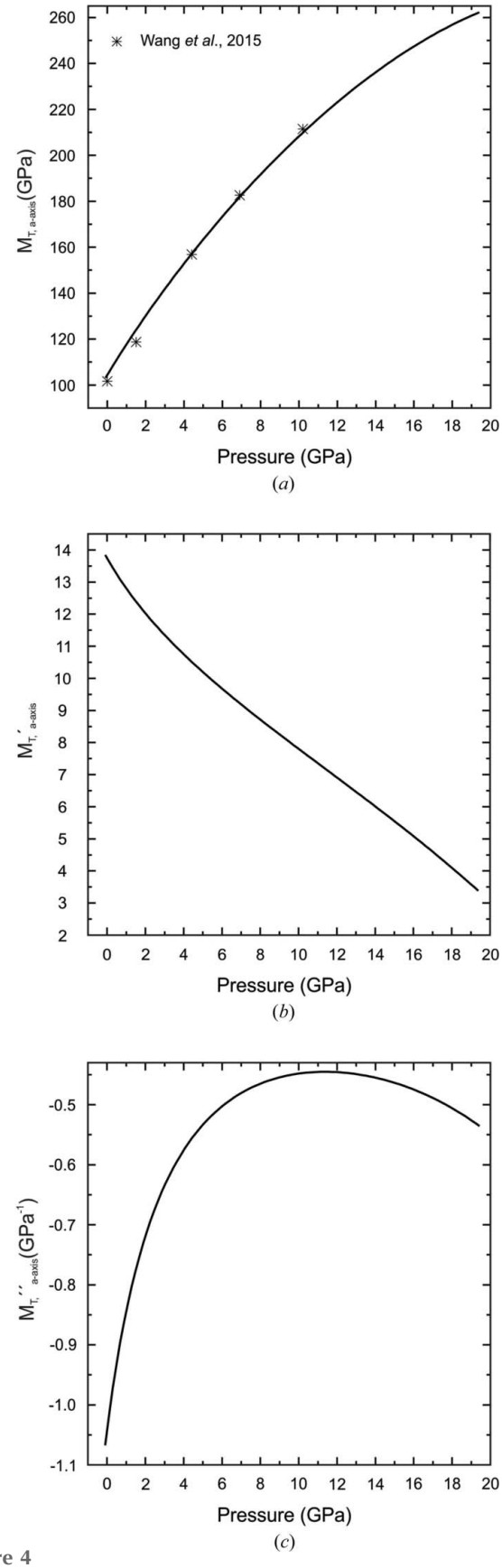

Figure 4
Plot of the EoS parameters of the fitted BM-4 derived from the *a*–*P* data: (*a*) axial modulus $M_T = -a_0(\delta P/\delta a)$, (*b*) the pressure derivative $M_T' = \delta M/\delta P$, and (*c*) the second derivative $M_T'' = \delta^2 M/\delta P^2$ as a function of pressure.

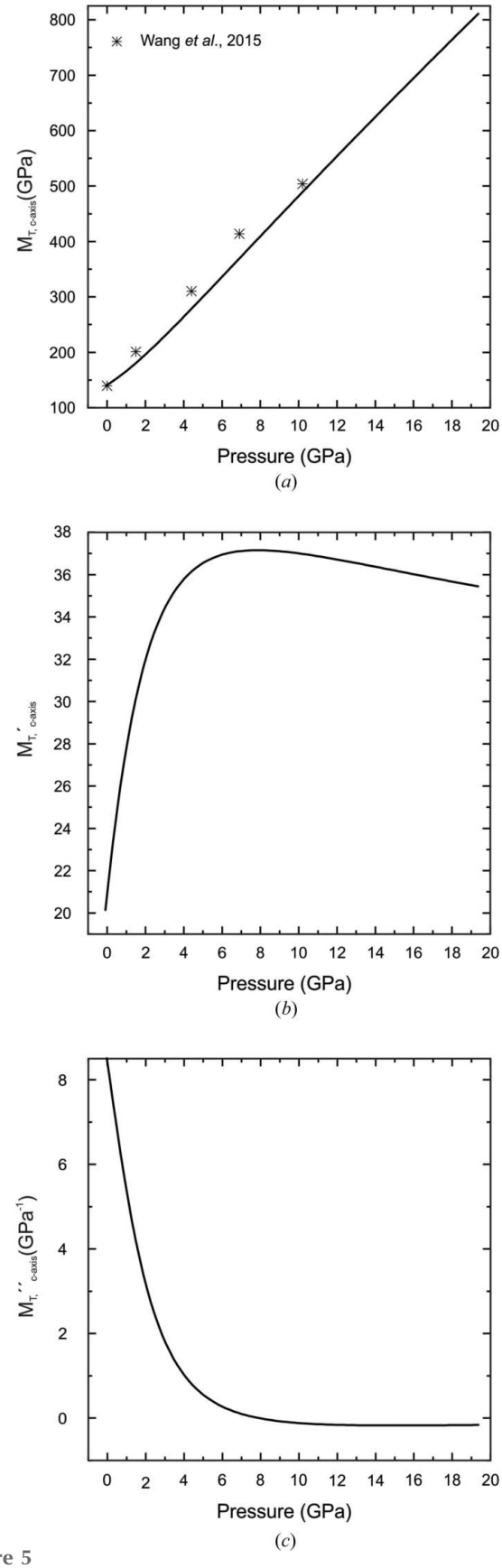

Figure 5
Plot of the EoS parameters of the fitted BM-4 derived from the *c*–*P* data: (*a*) axial modulus $M_T = -c_0(\delta P/\delta c)$, (*b*) the pressure derivative $M_T' = \delta M/\delta P$ and (*c*) the second derivative $M_T'' = \delta^2 M/\delta P^2$ as a function of pressure.

corresponds to an almost linear negative trend in its first pressure derivative M'_{aT} (Fig. 4*b*). Its second derivative M''_{aT} shows only a small variation with pressure (Fig. 4*c*). In contrast, the variation of the linear modulus M_{cT} of the *c* axis with pressure is almost linear, apart from the initial pressure range between atmospheric pressure and ~4 GPa (Fig. 5*a*). Corresponding to that, both its first and second pressure derivatives (M'_{cT} and M''_{cT}) show a strong initial variation up to about 4 GPa (Figs. 5*b* and 5*c*). Above 4 GPa the first pressure derivative M'_{cT} shows a slight decline, and the second derivative M''_{cT} approaches zero.

As already mentioned above, the compressibility of the *a* axis is at least two times larger than the compressibility of the *c* axis (*cf.* Figs. 2, 4*a* and 5*a*). At atmospheric pressure the ratio of M_{cT}/M_{aT} is 1.3, and it increases with pressure to a value of 3.1 at a pressure of 19 GPa. The different response to applied pressure of the *a* and *c* axes can be explained by the compression mechanism of the α-quartz structure (Sowa, 1988; Levien *et al.*, 1980; Hazen *et al.*, 1989; Glinnemann *et al.*, 1992; d'Amour *et al.*, 1979; Kim-Zajonz *et al.*, 1999). α-Quartz is built up by a framework of corner-shared SiO_2 tetrahedra, forming a pair of spiral chains running along the *c* axis. At the beginning of the compression process the Si—O—Si angles and the inter-tetrahedral O—O and Si—Si distances decrease, resulting in a tilting of the tetrahedra. This mechanism generally leads to a larger compressibility of the *a* axis compared to the *c* axis. During further compression, the O atoms along the *c* axis get closer and the packing of the O atoms is arranged towards a cubic *I*-centered framework, resulting in a stiffening of the *c* axis.

This compression mechanism leads to the volume compressibility plotted in Fig. 6. The bulk modulus K_T shows a curvature (Fig. 6*a*). Its first pressure derivative K'_T exhibits an initial curvature up to about 8 GPa, followed by an almost linear decrease (Fig. 6*b*), corresponding to an initial variation in the second derivative K''_T up to 8 GPa, and a subsequent stagnation (Fig. 6*c*). The initial high degree of compressional flexibility in the framework structure due to the rotational

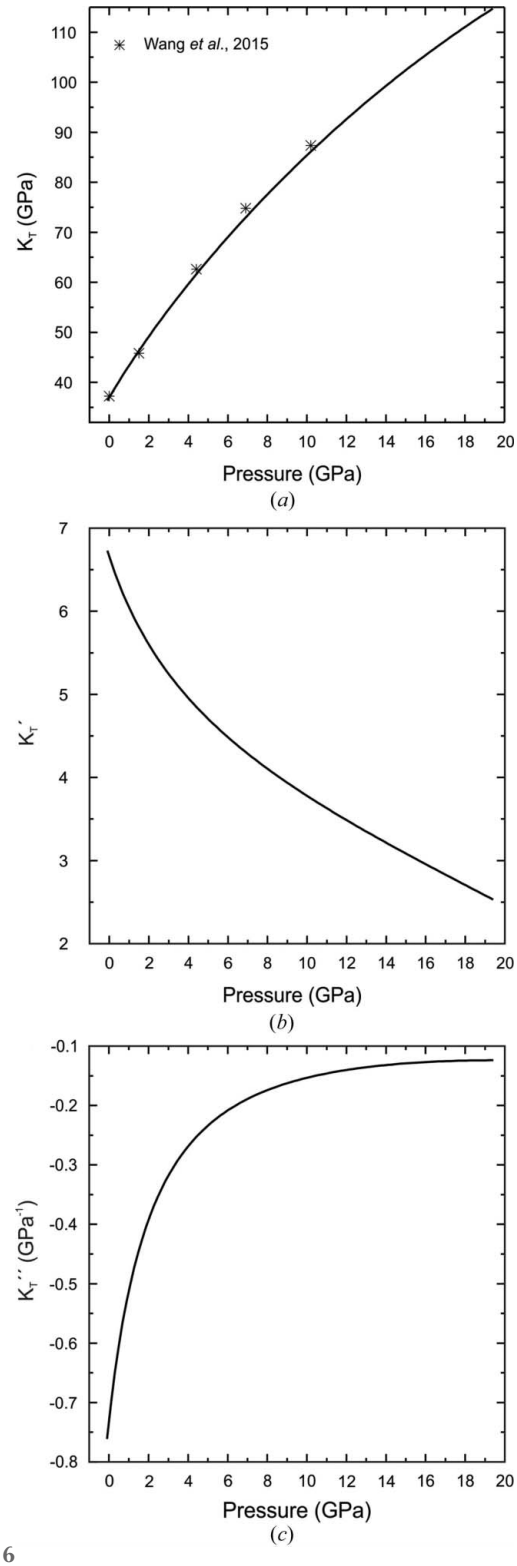

Figure 6
Plot of the EoS parameters of the fitted BM-4 derived from the *P*–*V* data: (*a*) bulk modulus $K_T = -V_0(\delta P/\delta V)$, (*b*) the pressure derivative $K'_T = \delta K/\delta P$ and (*c*) the second derivative $K''_T = \delta^2 K/\delta P^2$ as a function of pressure.

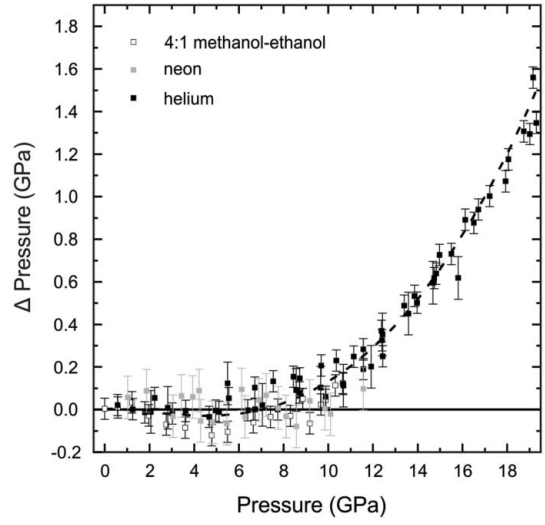

Figure 7
Plot of the differences in pressure ($\Delta P = P_{(\text{Angel } et\ al.,\ 1997)} - P_{(\text{this study})}$) as a function of pressure derived by ruby luminescence. The dashed line represents the reference line of the pressures determined after Angel *et al.* (1997). Symbols indicating the different pressure media correspond to those used in Fig. 1.

Table 4
Isothermal axial moduli M_{T0} of α-quartz at room pressure and temperature.

Author	Method	M_{T0} (a axis) (GPa)	M_{T0} (c axis) (GPa)
McSkimin *et al.* (1965)	Ultrasonic measurement	101.97†	136.96†
McWhan (1967)	X-ray diffraction	101.88	136.87
Wang *et al.* (1992)	Ultrasonic measurement	98.10†	139.24†
Angel *et al.* (1997)	X-ray diffraction	105.0 (5)	142.6 (1.0)
Heyliger *et al.* (2003)	Ultrasound spectroscopy	101.98†	137.16†
Choudhury & Chaplot (2006)	Density functional theory‡	102.84†	150.56†
Calderon *et al.* (2007)	Ultrasonic measurement	102.61†	136.34†
Kimizuka *et al.* (2007)	Density functional theory‡	94.49†	123.83†
Lakshtanov *et al.* (2007)	Brillouin spectroscopy	102.70†	137.81†
Tarumi *et al.* (2007)	Ultrasound spectroscopy	101.98†	136.48†
Wang *et al.* (2015)	Brillouin spectroscopy	101.63†	139.67†
This study	X-ray diffraction	104.5 (8)	141 (3)

† The isothermal axial moduli are derived from $M_T = M_S(\text{Reuss})/\{1 + \alpha_V\alpha_i[K_S(\text{Reuss})/C_P]T\}$, with $\alpha_V = 3.46 \times 10^{-5}\ \text{K}^{-1}$, $\alpha_1 = 1.36 \times 10^{-5}\ \text{K}^{-1}$, $\alpha_3 = 0.72 \times 10^{-5}\ \text{K}^{-1}$ obtained by fitting the data of Carpenter & Salje (1998) and $C_P = 0.00194\ \text{GPa K}^{-1}$, derived from $C_P = 746.3\ (1)\ \text{J kg}^{-1}\ \text{K}^{-1}$ (Hemingway, 1987). The adiabatic bulk modulus M_S(Reuss) is calculated from the given C_{ij} by $\beta_a = (C_{33} - C_{13})/(C_{11} + C_{12})C_{33} - 2C_{13}^2$ and $\beta_c = C_{11} + C_{12} - 2C_{13}/[(C_{11} + C_{12})C_{33} - 2C_{13}^2]$; $M_S = 1/\beta$. ‡ Zero temperature.

freedom of the structural units turns into a lower compressibility of the nearly close-packed oxygen configuration. As a result of the changing compression mechanism it is important to measure the entire pressure range to derive the compressibility adequately. The data of Angel *et al.* (1997), measured up to 8.9 GPa, did not show the necessity of an expansion to BM-4. The volume-compressibility parameters of their study derived by BM-4 lie within the s.u. values of the parameters derived by BM-3. Moreover the goodness of fit χ^2_w as well as $|P_{obs} - P_{calc}|$ does not improve using an extended BM equation.

As shown in this study α-quartz approaches structural instability close to the pressure regime of critical transformation or amorphization (>18 GPa). Therefore, elastic softening phenomena characterized by an increase in compressibility associated with structural transitions reported for various examples of pressure-induced phase transformations (*e.g.* Miletich *et al.*, 2014) could be expected. The feature of the elastic softening effect is the pronounced development of small or even negative values of K'_T. Neither the variation of the volume bulk modulus (Fig. 6*a*) nor that of the axial bulk modulus of the c axis (Fig. 5*a*) nor that of its pressure derivatives (Figs. 5*b* and 6*b*) gives evidence for any significant effect of elastic softening observable in the data presented here. The a axis shows the onset of elastic softening. The first pressure derivative of its axial bulk modulus decreases with pressure, develops to small values (Fig. 4*b*) and indicates the trend to negative values at pressures above the amorphization. However, as the softening process is only at the beginning at the point where quartz transforms, bulk elastic softening is not the driving force for the transformation, in agreement with theoretical models (*e.g.* Binggeli & Chelikowsky, 1992; Binggeli *et al.*, 1994; Choudhury & Chaplot, 2006).

5. Conclusion

The experimental study presented here, which encompasses several high-pressure measurements of α-quartz in 4:1 methanol–ethanol, neon and helium, shows that the choice of pressure medium does not influence the compression behavior of this material. The lack of significant pressure-induced intercalation of fluid components into the structure allows the application of the derived EoS parameters for pressure calibration, independent of the hydrostatic pressure medium used. The series of high-precision investigations carried out in this study have been extended up to 19 GPa and show that the parameters derived by Angel *et al.* (1997) need to be reconsidered with respect to the order of truncation of the used Birch–Murnaghan formalism. With this study we provide a new calibration of the pressure standard α-quartz over its entire stability range. We derived precise EoS parameters and proved that an extension to a fourth-order Birch–Murnaghan EoS is required to describe the compressibility of α-quartz properly. Employing these parameters to derive the pressure, the uncertainty is 0.004 GPa at 1 GPa, 0.006 GPa at 5 GPa, 0.009 GPa at 10 GPa, 0.012 GPa at 15 GPa and 0.013 GPa at 19 GPa with an average s.u. of the volume of about 0.0001%.

Acknowledgements

We thank Peter Kainzbauer for making available unpublished high-pressure data of quartz in the argon pressure medium and Thomas Pippinger for technical assistance. RM acknowledges the financial support of the University of Vienna through grant BE532003 and AK and DMT acknowledge the support of the ERC advanced grant 227893 'DEEP' funded *via* the EC Seventh Framework Programme. Finally we thank the two reviewers for their valuable suggestions and great effort, which significantly improved the manuscript.

References

Amour, H. d', Denner, W. & Schulz, H. (1979). *Acta Cryst.* B**35**, 550–555.
Angel, R. J. (1993). *J. Phys. Condens. Matter*, **5**, L141–L144.
Angel, R. J., Allan, D. R., Miletich, R. & Finger, L. W. (1997). *J. Appl. Cryst.* **30**, 461–466.
Angel, R. J., Bujak, M., Zhao, J., Gatta, G. D. & Jacobsen, S. D. (2007). *J. Appl. Cryst.* **40**, 26–32.
Angel, R. J. & Finger, L. W. (2011). *J. Appl. Cryst.* **44**, 247–251.
Angel, R. J., Gonzalez-Platas, J. & Alvaro, M. (2014). *Z. Kristallogr.* **229**, 405–419.
Bell, P. M. & Mao, H. K. (1981). *Carnegie Inst. Annu. Rep. Geophys. Lab.* **80**, 404–406.
Binggeli, N. & Chelikowsky, J. R. (1992). *Phys. Rev. Lett.* **69**, 2220–2223.
Binggeli, N., Keskar, N. R. & Chelikowsky, J. R. (1994). *Phys. Rev. B*, **49**, 3075–3081.
Birch, F. (1947). *Phys. Rev.* **71**, 809–824.
Boehler, R. & De Hantsetters, K. (2004). *High. Pressure Res.* **24**, 391–396.
Böhler, R. & Arndt, J. (1974). *Contrib. Miner. Petrol.* **48**, 149–152.
Calderon, E., Gauthier, M., Decremps, F., Hamel, G., Syfosse, G. & Polian, A. (2007). *J. Phys. Condens. Matter*, **19**, 436228.
Carpenter, M. A. & Salje, E. K. H. (1998). *Eur. J. Miner.* **10**, 693–812.

Chelikowsky, J. R., Troullier, N. & Martins, J. L. (1991). *Phys. Rev. Lett.* **44**, 489–497.

Chervin, J. C., Canny, B. & Mancinelli, M. (2001). *High. Pressure Res.* **21**, 305–314.

Choudhury, N. & Chaplot, S. L. (2006). *Phys. Rev. B*, **73**, 094304.

Datchi, F., LeToullec, R. & Loubeyre, P. (1997). *J. Appl. Phys.* **81**, 3333–3339.

Demuth, T., Jeanvoine, Y., Hafner, J. & Ángyán, J. G. (1999). *J. Phys. Condens. Matter*, **11**, 3833–3874.

Dewaele, A. & Loubeyre, P. (2007). *High. Pressure Res.* **27**, 419–429.

Di Pomponio, A. & Continenza, A. (1993). *Phys. Rev. Lett.* **48**, 12558–12565.

Dorfman, S. M., Prakapenka, V. B., Meng, Y. & Duffy, T. S. (2012). *J. Geophys. Res.* **117**, 1–15.

Glinnemann, J., King, H. E. Jr, Schulz, H., Hahn, T., La Placa, S. J. & Dacol, F. (1992). *Z. Kristallogr.* **198**, 177–212.

Gregoryanz, D., Hemley, R. J., Mao, H. K. & Gillet, P. (2000). *Phys. Rev. Lett.* **84**, 3117–3120.

Haines, J., Cambon, O., Levelut, C., Santoro, M., Gorelli, F. & Garbarino, G. (2010). *J. Am. Chem. Soc.* **132**, 8860–8861.

Haines, J., Léger, J. M., Gorelli, F. & Hanfland, M. (2001). *Phys. Rev. Lett.* **87**, 155503.

Hamann, D. R. (1996). *Phys. Rev. Lett.* **76**, 660–663.

Hamilton, W. C. & Ibers, J. A. (1974). *International Tables for X-ray Crystallography*, Vol. IV, pp. 273–284. Birmingham: Kynoch Press.

Hazen, R. (1983). *Science*, **219**, 1065–1067.

Hazen, R. M. & Finger, L. W. (1981). *J. Appl. Cryst.* **14**, 234–236.

Hazen, R. & Finger, L. (1984). *J. Appl. Phys.* **56**, 1838–1840.

Hazen, R. M., Finger, L. W., Hemley, R. J. & Mao, H. K. (1989). *Solid State Commun.* **72**, 507–511.

Hemingway, B. S. (1987). *Am. Miner.* **72**, 273–279.

Hemley, R. J., Jephcoat, A. P., Mao, H. K., Ming, L. C. & Manghnani, M. H. (1988). *Nature*, **334**, 52–54.

Heyliger, P., Ledbetter, H. & Kim, S. (2003). *J. Acoust. Soc. Am.* **114**, 644–650.

Holm, B. & Ahuja, R. (1999). *J. Chem. Phys.* **111**, 2071–2074.

Jacobsen, S. D., Holl, C. M., Adams, K. A., Fischer, R. A., Martin, E. S., Bina, C. R., Lin, J.-F., Prakapenka, V. B., Kubo, A. & Dera, P. (2008). *Am. Mineral.* **93**, 1823–1828.

Jayaraman, A., Wood, D. L. & Maines, R. G. Sr (1987). *Phys. Rev. B*, **35**, 8316–8321.

Jorgensen, J. D. (1978). *J. Appl. Phys.* **49**, 5473–5478.

Kantor, I., Prakapenka, V., Kantor, A., Dera, P., Kurnosov, A., Sinogeikin, S., Dubrovinskaia, N. & Dubrovinsky, L. (2012). *Rev. Sci. Instrum.* **83**, 125102.

Kimizuka, H., Ogata, S., Li, J. & Shibutani, Y. (2007). *Phys. Rev. B*, **75**, 054109.

Kim-Zajonz, J., Werner, S. & Schulz, H. (1999). *Z. Kristallogr.* **214**, 324–330.

Kingma, K. J., Hemley, R. J., Mao, H. K. & Veblen, D. R. (1993). *Phys. Rev. Lett.* **70**, 3927–3930.

Kingma, K. J., Meade, C., Hemley, R. J., Mao, H. K. & Veblen, D. R. (1993). *Science*, **259**, 666–669.

Klotz, S., Chervin, J.-C., Munsch, P. & Le Marchand, G. (2009). *J. Phys. D Appl. Phys.* **42**, 075413.

Knittle, E. (1995). *Mineral Physics and Crystallography, A Handbook of Physical Constants*, AGU Reference Shelf 2, edited by T. J. Ahrens, pp. 98–142. Washington, DC: American Geophysical Union.

Kurnosov, A., Kantor, I., Boffa-Ballaran, T., Lindhardt, S., Dubrovinsky, L., Kuznetsov, A. & Zehnder, B. H. (2008). *Rev. Sci. Instrum.* **79**, 045110.

Lakshtanov, D. L., Sinogeikin, S. V. & Bass, J. D. (2007). *Phys. Chem. Miner.* **34**, 11–22.

Lee, Y., Vogt, T., Hriljac, J., Parise, J. & Artioli, G. (2002). *J. Am. Chem. Soc.* **124**, 5466–5475.

Le Page, Y. & Donnay, G. (1976). *Acta Cryst.* B**32**, 2456–2459.

Levien, L., Prewitt, C. T. & Weidner, D. J. (1980). *Am. Mineral.* **65**, 920–930.

Lewis, J., Schwarzenbach, D. & Flack, H. D. (1982). *Acta Cryst.* A**38**, 733–739.

Lv, H., Yao, M., Li, Q., Liu, R., Liu, B., Lu, S., Jiang, L., Cui, W., Liu, Z., Liu, J., Chen, Z., Zou, B., Cui, T. & Liu, B. (2012). *J. Appl. Phys.* **111**, 1–5.

Mao, H. K., Xu, J. & Bell, P. M. (1986). *J. Geophys. Res. Solid Earth*, **91**, 4673–4676.

McSkimin, H. J., Andreatch, P. Jr & Thurston, R. N. (1965). *J. Appl. Phys.* **36**, 1624–1632.

McWhan, D. B. (1967). *J. Appl. Phys.* **38**, 347–352.

Miletich, R., Allan, D. R. & Kuhs, W. F. (2000). *High-Temperature and High-Pressure Crystal Chemistry*, Reviews in Mineralogy and Geochemistry, Vol. 41, edited by R. M. Hazen & R. T. Downs, pp. 445–520. Washington, DC: Mineralogical Society of America.

Miletich, R., Gatta, G. D., Willi, T., Mirwald, P. W., Lotti, P. & Merlini, M. (2014). *Am. Mineral.* **99**, 479–493.

Ming, L. C., Manghnani, M. H., Balogh, J., Qadri, S. B., Skelton, E. F. & Jamieson, J. C. (1983). *J. Appl. Phys.* **54**, 4390–4397.

Nakano, S., Sasaki, T., Takemura, K. & Watanabe, M. (1998). *Chem. Mater.* **10**, 2044–2046.

Systat Software (2007). *PeakFit*. Version 4.1.2. Systat Software UK Ltd, London, UK.

Perottoni, C. & da Jornada, J. (1997). *Phys. Rev. Lett.* **78**, 2991–2994.

Piermarini, G. J., Block, S. & Barnett, J. D. (1973). *J. Appl. Phys.* **44**, 5377–5382.

Sato, T., Takada, H., Yagi, T., Gotou, H., Okada, T., Wakabayashi, D. & Funamori, N. (2013). *Phys. Chem. Miner.* **40**, 3–10.

Schuster, B., Weikusat, C., Miletich, R., Trautmann, C., Neumann, R. & Fujara, F. (2010). *Phys. Rev. B*, **82**, 184110.

Scott, J. F. & Porto, S. P. S. (1967). *Phys. Rev.* **161**, 903–910.

Sowa, H. (1988). *Z. Kristallogr.* **184**, 257–268.

Talyzin, A. & Luzan, S. (2010). *J. Phys. Chem. C*, **114**, 7004–7006.

Talyzin, A., Sundqvist, B., Szabó, T., Dékány, I. & Dmitriev, V. (2009). *J. Am. Chem. Soc.* **131**, 18445–18449.

Tarumi, R., Nakamura, K., Ogi, H. & Hirao, M. (2007). *J. Appl. Phys.* **102**, 113508.

Trots, D. M., Kurnosov, A., Ballaran, T. B., Tkachev, S., Zhuravlev, K., Prakapenka, V., Berkowski, M. & Frost, D. J. (2013). *J. Geophys. Res. Solid Earth*, **118**, 5805–5813.

Trots, D. M., Kurnosov, A., Vasylechko, L., Berkowski, M., Boffa Ballaran, T. & Frost, D. J. (2011). *Phys. Chem. Miner.* **38**, 561–567.

Wang, J., Mao, Y., Jiang, F. & Duffy, T. S. (2015). *Phys. Chem. Miner.* **42**, 203–212.

Wang, Q., Saunders, G. A., Lambson, E. F., Tschaufeser, P., Parker, S. C. & James, B. J. (1992). *Phys. Rev. B*, **45**, 10242–10254.

Williams, Q., Hemley, R. J., Kruger, M. B. & Jeanloz, R. (1993). *J. Geophys. Res.* **98**, 22157–22170.

Yagi, T., Iida, E., Hirai, H., Miyajima, N., Kikegawa, T. & Bunno, M. (2007). *Phys. Rev. B*, **75**, 174115.